I&EC research
Industrial & Engineering Chemistry Research

pubs.acs.org/IECR

Article

Hydrothermal Synthesis of Sub-20 nm Amine-Functionalized MIL-101(Cr) Nanoparticles with High Surface Area and Enhanced CO_2 Uptake

Gang Han, Qihui Qian, Katherine Mizrahi Rodriguez, and Zachary P. Smith*

Cite This: *Ind. Eng. Chem. Res.* 2020, 59, 7888−7900

Read Online

ACCESS | Metrics & More | Article Recommendations | Supporting Information

ABSTRACT: An assortment of hydrothermal reactions of chromic(III) nitrate and 2-aminoterephthalic acid was systematically studied to yield high-quality amine-functionalized MIL-101(Cr) nanoparticles (MIL-101(Cr)-NH_2). A comprehensive understanding of the role that synthesis conditions and basic modulators have on the formation of MIL-101(Cr)-NH_2 in aqueous media was extracted and reported herein. With the aid of a NaOH modulator at optimized concentration, sub-20 nm MIL-101(Cr)-NH_2 nanoparticles were prepared with good yield, minimized particle agglomeration, and a high Brunauer−Emmett−Teller (BET) surface area of 2800 ± 200 m^2/g. To the best of our knowledge, these are the smallest particle sizes and the highest surface areas reported for directly synthesized MIL-101(Cr)-NH_2. Owing to their superior surface area and Lewis basic amine functionality, the MIL-101(Cr)-NH_2 nanoparticles exhibit a high CO_2 adsorption of up to 3.4 mmol/g at 288 K and 1 bar and a superior CO_2/N_2 selectivity of 26.5 at 308 K and 0.1 bar. A high isosteric heat of −54.6 kJ/mol for CO_2 adsorption implies the strong interaction between CO_2 and the amine-functionalized framework. The successful synthesis of sub-20 nm amine-functionalized MIL-101(Cr) nanoparticles offers a great opportunity to engineer advanced MIL-101(Cr)-based functional adsorbents and membranes for CO_2 capture and separation.

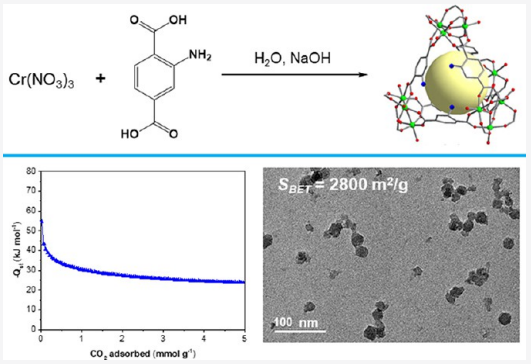

1. INTRODUCTION

Metal−organic frameworks (MOFs), assembled by the bonding of metal ions or clusters linked with polyfunctional organic molecules, have emerged as an intriguing class of crystalline porous materials.[1,2] The most attractive feature of MOFs is their unique combination of physicochemical properties, including but not limited to their well-ordered porous structures with a wide range of pore sizes and functionality, ultrahigh porosity, and enormous internal surface areas.[3,4] MOFs are eliciting attention in chemical and material sciences for their prospective applications in catalysis,[5,6] drug delivery,[7,8] sensing or recognition,[9] gas storage,[10] and separations.[11,12] Rational design and synthesis of MOF-based adsorbents and membranes with prescribed structural and functional features for carbon capture have been a particular focus.[10−13] The hybrid nature of MOFs provides almost infinite variability for manipulating the inorganic and organic building blocks to target specific CO_2 adsorption behavior either by introducing open metal sites (OMSs) and/or functional groups into the framework during synthesis or by modulating the properties of the MOF via postsynthetic modification.[3,4]

MIL-101(Cr) (MIL: Matérial Institut Lavoisier) is a terephthalate-based mesoporous MOF composed of trimeric chromium(III) octahedral clusters interconnected by 1,4-benzenedicarboxylates, resulting in an augmented MTN zeotype crystal structure.[14−16] The framework contains two types of mesoporous quasi-spherical cages with diameters of ∼29 and 34 Å, respectively. The smaller cages are accessible through pentagonal windows with a free opening of ∼12 Å, while the larger cages have both pentagonal and hexagonal windows with a ∼14.7 Å by 16 Å free aperture.[15,16] As a result of its highly porous structure, MIL-101(Cr) shows some of the highest Brunauer−Emmett−Teller (BET) and Langmuir surface areas for MOFs (4100 ± 200 and 5900 ± 300 m^2/g) and a giant cell volume of about 702 000 $Å^3$.[15,16] Approximately 3.0 mmol/g of Cr in this MOF exists as coordinatively unsaturated OMSs upon activation and removal of terminal water molecules from the Cr_3O trimers in the framework.[16] In addition, MIL-101(Cr) is thermally stable in air of up to 275 °C before decomposition and can withstand various organic solvents.[15,16] These remarkable properties make MIL-101(Cr) attractive for potential applications in heterogeneous catalysis,

Received: February 1, 2020
Revised: March 12, 2020
Accepted: March 22, 2020
Published: March 23, 2020

energy storage, water filtration, and gas separations as either adsorbents or molecular sieve fillers in composite membranes.[16−20]

As an isoreticular modification of MIL-101(Cr), amine-functionalized MIL-101(Cr) is potentially more attractive because the presence of amine groups on the pore walls not only helps improve affinity for particular molecules such as CO_2[21−24] but also provides a chemical anchor for post-synthetic modification.[25−27] A wide range of functional groups can be introduced into the framework through amine chemistry by which the performance of MIL-101(Cr) in many applications can be further improved.[28−31] However, the synthesis of functionalized MOFs is challenging because functionalized ligands are often incompatible with the conditions necessary for MOF assembly. For example, significant variations in reaction conditions can be expected when the ligand is changed from conventional terephthalic acid to 2-aminoterephthalic acid as the amine groups normally change the Brønsted acid−base properties, solubility, and thermal stability of the ligand.[32] Up to now, rather limited work on the direct synthesis of amine-functionalized MIL-101(Cr) has been reported in the open literature. Lin et al. reported a hydroxide-assisted synthesis of MIL-101(Cr)-NH_2 using 2-aminoterephthalic acid as the ligand at 150 °C for 12 h.[33] Jiang et al. demonstrated another hydrothermal method to prepare MIL-101(Cr)-NH_2 in pure water at a lower temperature of 130 °C for 24 h.[34] However, the majority of these studies were directed toward a detailed characterization of the products and their derivatives. The syntheses are briefly described, and a systematic investigation of the reaction parameters is missing. Of note, the reported MIL-101(Cr)-NH_2 particles have relatively large particle size with significant agglomerations and possess much lower surface area (i.e., 1675−2070 m^2/g) than that reported for the parent MIL-101(Cr) (i.e., 3000-4100 m^2/g for BET surface area).[15,16,35] Low surface area limits their gas uptake capacity, while severe particle agglomerations hinder scale-up and would further preclude the eventual formation of defect-free composite membranes, which require both small particles and limited agglomeration. To improve the physical and chemical properties of MIL-101(Cr)-NH_2 and expand its accessible applications to adsorption and membrane separations, it is critical to understand the influence of each parameter on MIL-101(Cr)-NH_2 crystal formation.

As illustrated in Figure 1, this work aims to synthesize high-quality amine-functionalized MIL-101(Cr) nanoparticles directly from the reaction of chromic nitrate and 2-aminoterephthalic acid in aqueous media. We systematically investigated the influence of reaction temperature and time, reagent concentration, and the basic modulators in the formation of MIL-101(Cr)-NH_2. The physical and chemical properties of the as-prepared nanoparticles were thoroughly characterized by X-ray diffraction (XRD), transmission electron microscopy (TEM), scanning electron microscopy (SEM), thermogravimetric analysis (TGA), Fourier transform infrared (FTIR) spectroscopy, X-ray photoelectron spectroscopy (XPS), and BET measurements. Using this extensive set of characterization tests, we summarize a comprehensive study pinpointing the role of incremental variations in composition and other process parameters like basic modulators on the direct synthesis of amine-functionalized MIL-101(Cr). Sub-20 nm MIL-101(Cr)-NH_2 nanoparticles with good yield, low particle agglomerations, and high surface areas are prepared,

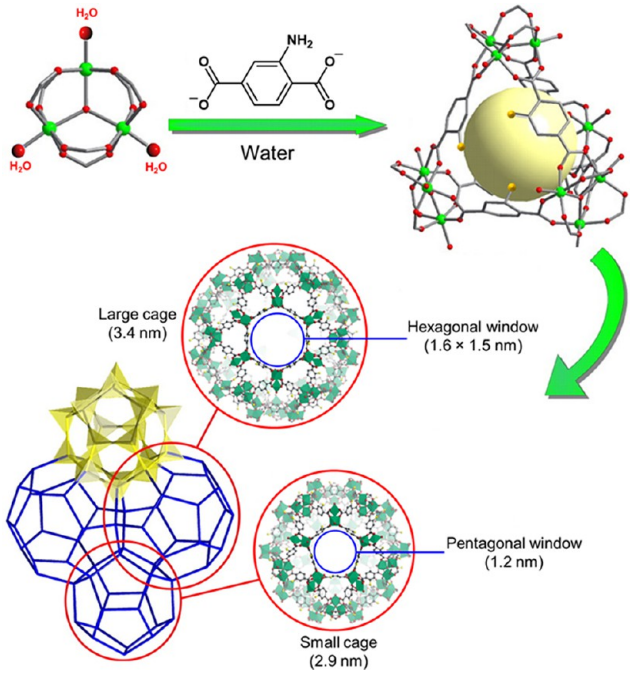

Figure 1. Schematic representation of the basic building units and crystal structure of MIL-101(Cr)-NH_2.[15,20] Small red atoms represent oxygen, large red atoms represent oxygen on H_2O, green atoms represent chromium, and yellow atoms represent nitrogen. Implicit carbons and hydrogens are not shown for clarity.

which exhibit great potential for application in CO_2 capture as adsorbents and fillers in composite membranes. The experimental insights from this study will also aid in the development of new MOF synthesis protocols and translate to the synthesis of other amine-functionalized MOFs.

2. EXPERIMENTAL AND CHARACTERIZATION METHODS

2.1. Materials. Chromium nitrate nonahydrate ($Cr(NO_3)_3·9H_2O$, 99.0%), terephthalic acid (H_2BDC, 99.0%), 2-aminoterephthalic acid (H_2N-H_2BDC, 99.0%), sodium hydroxide (NaOH, 97.0%), triethylamine (Et_3N, 99.5%), and sodium formate (SF) (HCOONa, 99.0%) were purchased from Sigma-Aldrich and used as received. Deionized water was used as the solvent for the syntheses. *N*,*N*-Dimethylformamide (DMF, 99.8%) and ethanol (EtOH, 99.9%) obtained from VWR were used as received as the solvents for particle purification.

2.2. Synthesis of MIL-101(Cr)-NH_2. The amine-functionalized MIL-101(Cr) nanoparticles, MIL-101(Cr)-NH_2, were synthesized via a one-pot hydrothermal reaction. In a typical synthesis, $Cr(NO_3)_3·9H_2O$ (252.1 mg, 0.63 mmol) and H_2N-H_2BDC (114.1 mg, 0.63 mmol) were dispersed in 10 mL deionized water and then sonicated for 1 h at room temperature, resulting in a violet-colored suspension. The suspension was then transferred into a 30 mL Teflon-lined stainless steel autoclave and heated at different temperatures for different times under autogenous pressure without stirring. Table S1 summarizes the detailed reaction conditions for each synthesis in pure water without any additives. For base-modulated syntheses, different amounts of NaOH, Et_3N, or HCOONa were added into the mixture of $Cr(NO_3)_3·9H_2O$ (252.1 mg, 0.63 mmol), H_2N-H_2BDC (114.1 mg, 0.63 mmol), and deionized water (10 mL) following the same procedure as

https://dx.doi.org/10.1021/acs.iecr.0c00535
Ind. Eng. Chem. Res. 2020, 59, 7888−7900

the modulator-free syntheses. The detailed reaction conditions for each synthesis with basic modulator are tabulated in Table S2. To study the influence of reagent concentration on MOF synthesis, the amounts of both $Cr(NO_3)_3{\cdot}9H_2O$ and H_2N-H_2BDC were doubled to 1.26 mmol and the volume of water was reduced to 7 mL, as shown in Table S3. After the reaction, the autoclave was left in the convection oven to naturally cool down to room temperature. The green precipitates were collected by centrifugation (rpm = 11 000, 120 min). The reported reaction yield based on chromium was calculated from three independent syntheses.

2.3. Synthesis of MIL-101(Cr). The parent MIL-101(Cr) benchmark was hydrothermally synthesized on the basis of a HF-free procedure reported by Bromberg and co-workers with minor changes.[36] In a typical reaction, $Cr(NO_3)_3{\cdot}9H_2O$ (2.0 g, 5.0 mmol) and H_2BDC (0.83 g, 5.0 mmol) were dispersed in 20 mL deionized water and then sonicated at room temperature for 1 h. The suspension was then transferred into a 30 mL Teflon-lined autoclave and kept at 218 °C for 15 h under autogenous pressure without stirring. After the reaction, the autoclave was naturally cooled down to room temperature and the green precipitates were collected by centrifugation (rpm = 11 000, 60 min).

2.4. Purification of MOF Particles. A comprehensive washing procedure was applied to purify the as-synthesized crude MIL-101(Cr)-NH_2 and MIL-101(Cr) particles. After each synthesis, the green precipitates were washed with 20 mL deionized water to remove any unreacted chromium salt and water-soluble additives. The green particles were subsequently washed with DMF 3 times at room temperature to eliminate the unreacted carboxylic acid ligand, after which the products were further washed with ethanol 3 times. For each washing step, 20 mL of fresh DMF and ethanol were used to disperse the particles, and the resulting suspension was indirectly sonicated for 12 h to remove the unreacted ligand and modulator remaining in the pores. The solid product was isolated by centrifugation (11 000 rpm and 120 min for MIL-101(Cr)-NH_2 and 60 min for MIL-101(Cr)). Finally, the purified particles were vacuum-dried at 130 °C for 12 h and then activated at 150 °C for 24 h before characterization.

2.5. Characterization. Powder XRD data were acquired on a Rigaku Smartlab multipurpose X-ray diffractometer with Cu Kα radiation (λ = 1.5406 Å) at a voltage of 45 kV and 200 mA. The XRD patterns were scanned over the angular range of 2−40° (2θ) with a step size of 0.1°. TEM images were obtained using an FEI Tecnai (G2 Spirit TWIN) multipurpose digital system operating at 120 kV. TEM samples were prepared by placing drops of the particle dispersion in ethanol on lacey carbon-coated 200 mesh copper grids (Electron Microscopy Sciences). A Zeiss Merlin high-resolution scanning electron microscope was used for particle morphological analysis. SEM samples were sputter-coated with a ∼6 nm layer of gold/palladium alloy using a Desk II cold sputter unit (Denton Vacuum LLC). The thermal stability analysis of the particles was conducted on a TGA 550 thermogravimetric analyzer in air at a heating rate of 10 °C/min under temperature ramp mode. The FTIR spectra in the range of 400−4000 cm^{-1} were collected by a Thermo Fisher FTIR6700 spectrometer in transmission mode using a resolution of 4 cm^{-1} with 32 scans. The elemental and chemical spectroscopic analyses were examined by XPS using a ULVAC-PHI Versaprobe II instrument with a monochromatic Al Kα X-ray source ($h\nu$ = 1486.6 eV). The X-ray source power was 50 W, and the beam spot size was 200 μm. Survey spectra and high-energy resolution spectra were taken with pass energies of 187.85 and 23.50 eV, respectively. All spectra were obtained with a photoelectron take-off angle of 45.0°. The nitrogen adsorption−desorption isotherms were measured on a Micromeritics 3Flex apparatus at 77 K. The Brunauer−Emmett−Teller (BET) surface areas were calculated over the range of relative pressures between 0.05 and 0.20. All BET tests were run in triplicate, and standard deviations are reported from three independent experiments. Single and representative BET isotherms are presented for figures in the text.

2.6. Gas Adsorption Measurements. The CO_2 and N_2 adsorption isotherms of the MOF particles were measured using gases of ultrahigh purity from Airgas on a Micromeritics 3Flex apparatus at different temperatures and pressures. An in situ water bath with a heating and cooling chiller was used to precisely control the temperature of the sample tube. In a typical procedure, a vacuum-dried sample (∼100−150 mg) was loaded into the glass analysis tube, which was then transferred to a degas port to be heated and evacuated, including an initial ramp to 100 °C at 10 °C/min, a hold at 100 °C for 30 min, and a final ramp to 150 °C at 10 °C/min, where the temperature was held for 12 h. After degassing, the sample tube was backfilled with N_2 and then transferred to the analysis port. During the tests, the equilibrium interval time for each measuring pressure point was set to 300 s to ensure equilibrium was reached.

The relationship of adsorption amount versus gas bulk pressure at equilibrium was determined using the Langmuir−Freundlich fit for the isotherms[25,33,37]

$$\frac{N}{N_m} = \frac{B \times P^{(1/t)}}{1 + B \times P^{(1/t)}} \tag{1}$$

where N represents the uptake amount at a certain equilibrium pressure (P), N_m is the theoretical maximum uptake at saturation, and both B and t are the equation constants. To obtain accurate pressure, P, corresponding to the same adsorption amount, the above equation can be rearranged to

$$P = \left(\frac{N/N_m}{B - B \times N/N_m}\right)^t \tag{2}$$

The ideal selectivity (α) of CO_2/N_2 at a certain pressure was calculated using the following equation

$$\alpha = \frac{N_{CO_2}}{N_{N_2}} \tag{3}$$

The isosteric heat values for CO_2 adsorption were calculated using the Clausius−Clapeyron equation[38,39]

$$\frac{d \ln P}{d(1/T)} = -\frac{Q_{st}}{R} \tag{4}$$

3. RESULTS AND DISCUSSION

3.1. Synthesis of MIL-101(Cr)-NH_2 in Pure Water. Direct synthesis of MIL-101(Cr)-NH_2 from $Cr(NO_3)_3{\cdot}9H_2O$ and H_2N-H_2BDC was first performed in pure water without using any additives. As summarized in Table S1, the influence of reaction temperature was studied by increasing the reaction temperature from 100 to 180 °C in nine independent experiments carried out for a reaction time of 24 h.

https://dx.doi.org/10.1021/acs.iecr.0c00535
Ind. Eng. Chem. Res. 2020, 59, 7888−7900

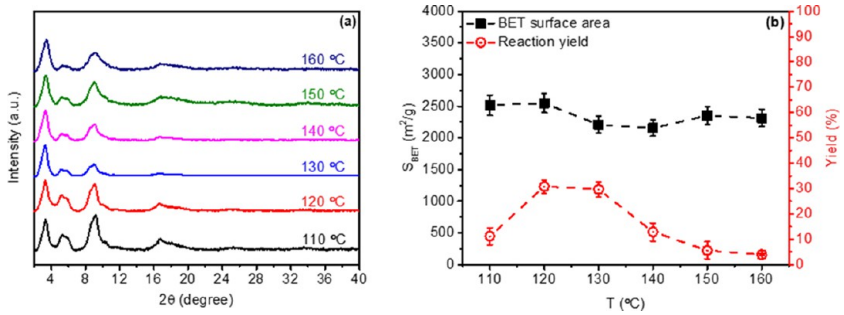

Figure 2. Powder XRD patterns (a) and BET surface areas and reaction yields (b) of MIL-101(Cr)-NH_2 nanoparticles synthesized at different temperatures for 24 h in pure water.

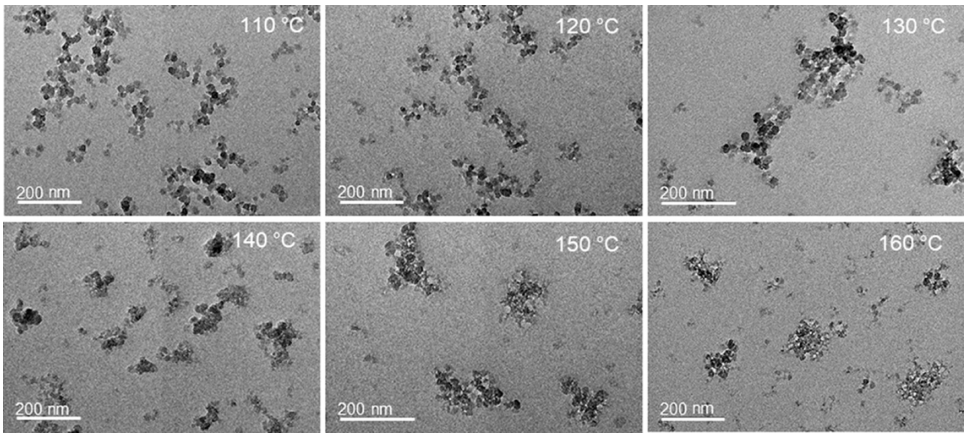

Figure 3. TEM images of MIL-101(Cr)-NH_2 nanoparticles synthesized at different temperatures for 24 h in pure water.

Additionally, the influence of reaction time was studied at 120 °C for four independent experiments, varying the reaction time between 6 and 48 h. The molar ratio and the exact amount of starting materials were kept constant. Conclusions are derived from these screening experiments based on powder XRD, TEM morphology and particle size analysis, reaction yield, and BET surface area of the resulting particles.

Variations in the reaction temperature strongly influence the particle formation and yield of MIL-101(Cr)-NH_2. After completing 24 h reactions at temperatures of up to 100 °C, no MOF particles formed and the H_2N-H_2BDC ligand remained in the mixture (see Figure S1a). Reactions performed at higher temperatures of 110−160 °C yielded green particles (see Figure S2a) with the same characteristic XRD peaks as to those for MIL-101(Cr) MOFs (see Figure 2a), suggesting the successful formation of MIL-101(Cr)-NH_2. When the temperature was further increased to 170 °C and 180 °C, however, an amorphous phase appeared on the X-ray spectra (see Figure S3), independent of the reaction time. This finding implies the potential degradation of the MOF building blocks at higher temperatures (see Figure S2a).

The yield of MIL-101(Cr)-NH_2 particles was also directly influenced by reaction temperatures. As depicted in Figure 2b, the reaction yield is relatively low at 110 °C and rapidly increases with the increase of temperature, reaching a yield almost 3 times higher than that of 110 °C at 120 and 130 °C. A further increase in reaction temperature leads to a significant drop in reaction yield, and an exceedingly low yield was obtained at 160 °C. One possible explanation for the resulting amorphous phase and the decay in yield at high temperatures is the thermal stability of the 2-aminoterephthalic acid ligand. At low temperatures, such as 100 °C, the solubility of the ligand is low,[40] resulting in poor proton dissociation from the carboxylic acids to provide enough 2-aminoterephthalate ions for MOF crystal formation. As the temperature is increased, ligand solubility improves and the equilibrium shifts toward the dissociated products, providing the required anions needed for particle formation and growth. As a result, the reaction yield increases with the increase of reaction temperature. However, 2-aminoterephthalic acid begins to degrade at higher temperatures due to its relatively low thermal stability,[32] resulting in a significant decline in yield. As shown in Figures S2a and S3, the reaction solution darkens and purely amorphous XRD patterns result when the reaction temperature is beyond 160 °C.

Figures 2b and S4 show that all MIL-101(Cr)-NH_2 particles formed at 110−160 °C have similar BET surface areas, ranging from 2200 ± 100 to 2500 ± 200 m^2/g. The low surface areas of 600 ± 50 and 400 ± 70 m^2/g for the products formed at 170 °C and 180 °C further confirm their amorphous structure (see Figure S5). Figures 3 and S6−S13 present the TEM images of the MIL-101(Cr)-NH_2 particles synthesized at different temperatures. In general, the sizes of the particles are very small at approximately 20 nm, which explains their broad XRD diffraction peaks. At a relatively high temperature of 160 °C, particle agglomeration and trace amounts of an apparent amorphous phase were observed in the particles. Further increases in temperature to 170 °C and 180 °C resulted in significantly larger aggregates with irregular shapes, as clearly observed from the TEM images, which is in good agreement with their amorphous XRD patterns and low BET surface areas.

https://dx.doi.org/10.1021/acs.iecr.0c00535
Ind. Eng. Chem. Res. 2020, 59, 7888−7900

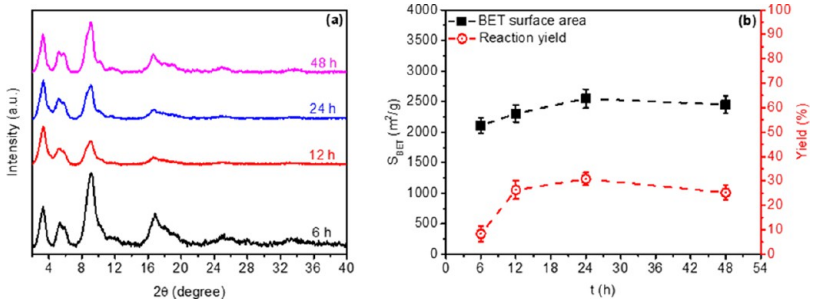

Figure 4. Powder XRD patterns (a) and BET surface areas and reaction yields (b) of MIL-101(Cr)-NH_2 synthesized at 120 °C for various times in pure water.

The influence of reaction time on MIL-101(Cr)-NH_2 formation was investigated in four separate reactions performed at a constant temperature of 120 °C for either 6, 12, 24, or 48 h. As shown in Figures 4a and S2b, reaction time shows a negligible effect on the crystalline structure of the particles, and MIL-101(Cr)-NH_2 is formed for all times considered in the range of 6−48 h. However, reaction time directly affected the particle yield and BET surface area. As displayed in Figure 4b, the reaction yield is relatively low for a short reaction period of 6 h, and some unreacted 2-aminoterephthalic acid ligand is observed in the resulting reaction mixture (see Figure S1b). With the increase of reaction time, the yield rapidly increases and reaches the highest value of 31% at 24 h. Further increasing the reaction time shows a slight change in the reaction yield. This finding suggests that the dissociation of protons in 2-aminoterephthalic acid in water is relatively slow, thus making this step the rate-determining step for crystal formation. A similar trend was observed for the BET surface area, where a lower surface area of 2100 ± 100 m^2/g was obtained for the 6 h reaction and a higher surface area of 2500 ± 200 m^2/g was obtained for the 24 h reaction (see Figures 4b and S14). TEM images in Figures 5 and S15−S17 show that reaction times below 24 h

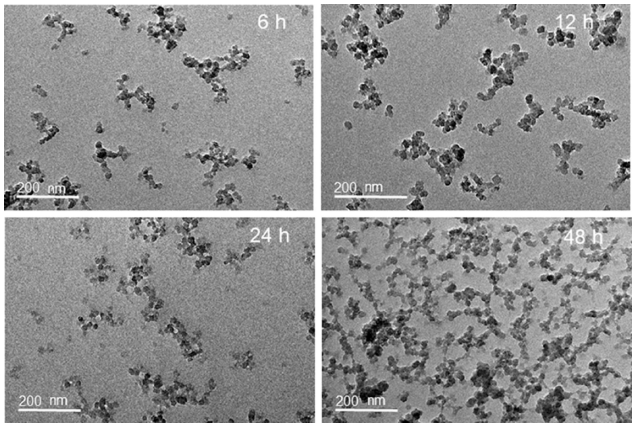

Figure 5. TEM images of MIL-101(Cr)-NH_2 nanoparticles synthesized at 120 °C for various times in pure water.

have a minor effect on particle size and all of the particles are less than 20 nm. However, when the reaction time is extended to 48 h, the nanoparticles begin to form an interconnected network and large aggregates, which explains the slight drop in their surface area (e.g., 2400 ± 200 m^2/g).

Having defined the optimal temperature and reaction time necessary for MIL-101(Cr)-NH_2 formation, we were interested in studying the effect of reagent concentration on the particle yield, size, morphology, and surface area. Insight in this respect could be useful for scaling up the synthesis of MIL-101(Cr)-NH_2, which often results in unpredictable changes in crystallinity. Additionally, since our earlier results suggested that ligand dissociation is the rate-limiting step for this reaction, we hypothesized that increased reactant concentration would not affect particle formation since the ligand had already reached its solubility limit in earlier experiments. As summarized in Table S3, two syntheses with different concentrations of $Cr(NO_3)_3{\cdot}9H_2O$ and H_2N-H_2BDC were conducted at 130 °C for 24 h, and the molar ratio of $Cr(NO_3)_3{\cdot}9H_2O$/H_2N-H_2BDC was kept at 1.0. Figure 6 and Table S3 show that the two reactions have similar reaction yield and the particles display the typical XRD patterns of MIL-101(Cr)-NH_2 crystals. MIL-101(Cr)-NH_2 formed with higher reagent concentration possesses a BET surface area of 2100 ± 200 m^2/g, which is remarkably similar to that of MIL-101(Cr)-NH_2 particles reported in the literature (i.e., 2070 m^2/g),[34] but slightly lower than that of the MIL-101(Cr)-NH_2 synthesized at lower concentrations (e.g., 2200 ± 100 m^2/g). This slight difference in the surface area can be attributed to the slight increase in the particle size and agglomeration that is observed when the reagent concentration is increased (see Figures S8 and S18). Therefore, while solubility of the ligand still appears to be the rate-limiting step for particle growth, there is a slight dependence on concentration with particle size. Clearly, these experiments demonstrate that the synthesis of MIL-101(Cr)-NH_2 can be scaled up without causing a significant change in particle yield and surface area, which are likely related to the low solubility of the H_2N−H_2BDC ligand in water.

3.2. Synthesis of MIL-101(Cr)-NH_2 in Water with the Presence of Basic Modulators. On a fundamental level, the solubility and dissociation of the carboxylic acid ligand in the solvent employed for this reaction are crucial for MOF formation. In view of the low solubility of the H_2N−H_2BDC ligand in water, the addition of basic modulators in the aqueous mixture would shift the equilibrium of deprotonation of H_2N−H_2BDC and increase its solubility, which in turn could significantly affect the nucleation and growth of MIL-101(Cr)-NH_2 particles by providing a larger amount of 2-aminoterephthalate ions for crystal formation.[41,42] As a result, we further investigated the reaction system of $Cr(NO_3)_3{\cdot}9H_2O$, H_2N−H_2BDC, water and added basic modulators.

As summarized in Table S2, the influence of reaction temperature was examined using NaOH as the probe modulator with a NaOH/H_2N−H_2BDC molar ratio of 1.0. The XRD data in Figure 7a confirms that MIL-101(Cr)-NH_2 is

https://dx.doi.org/10.1021/acs.iecr.0c00535
Ind. Eng. Chem. Res. 2020, 59, 7888−7900

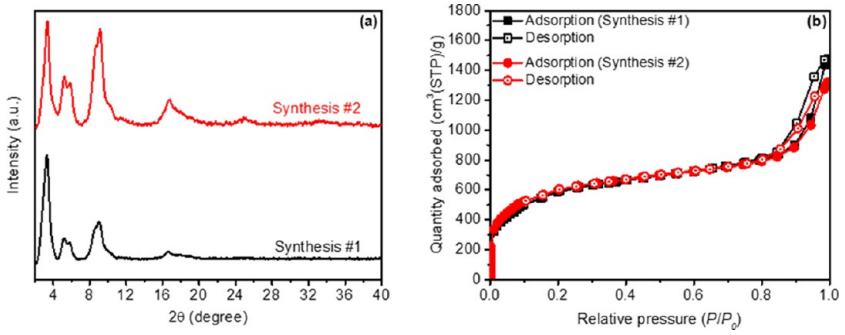

Figure 6. Powder XRD patterns (a) and N_2 adsorption−desorption isotherms at 77 K (b) for MIL-101(Cr)-NH_2 synthesized at 130 °C for 24 h using different reactant concentrations. The detailed conditions for both syntheses are summarized in Table S3.

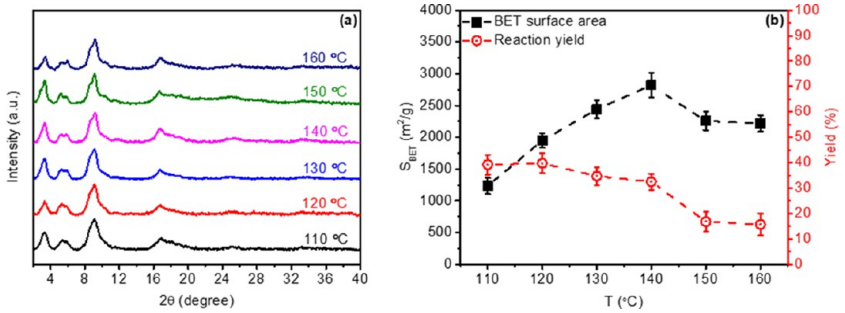

Figure 7. Powder XRD patterns (a) and BET surface areas and reaction yields (b) of MIL-101(Cr)-NH_2 nanoparticles synthesized at different temperatures for 24 h using a NaOH modulator with a NaOH/H_2N−H_2BDC molar ratio of 1.0 in water.

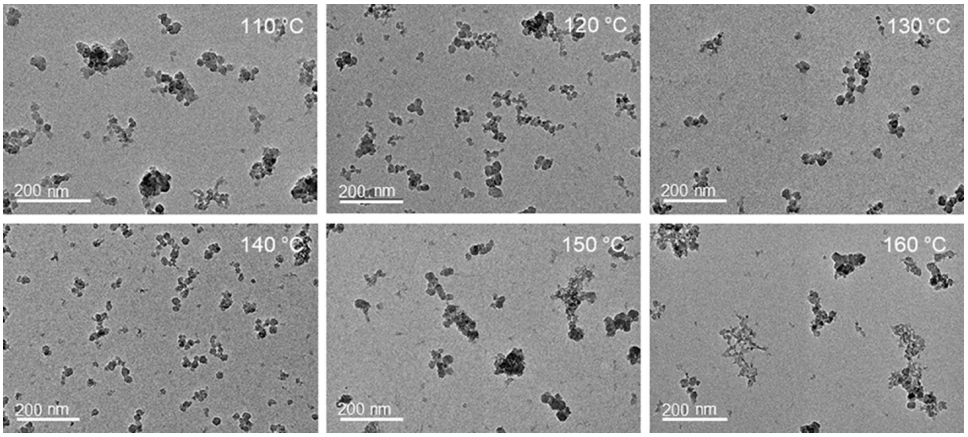

Figure 8. TEM images of MIL-101(Cr)-NH_2 nanoparticles synthesized at different temperatures for 24 h using a NaOH modulator with a NaOH/H_2N−H_2BDC molar ratio of 1.0 in water.

formed at 110−160 °C, which is similar to the syntheses in pure water, suggesting that the addition of NaOH has no influence on the thermal stability of H_2N−H_2BDC ligand. However, Figure 7b shows that the reaction yield at each temperature is significantly improved with the addition of NaOH. For example, the yield at a low reaction temperature of 110 °C is approximately 4 times higher than that of the synthesis without the NaOH modulator (see Figure 2b). The enhancement in reaction yield is attributed to the improved deprotonation of the carboxylic acid in H_2N−H_2BDC in water by NaOH. Similar to the previous observation in syntheses without a modulator, a rapid decrease in reaction yield is observed with the increase of reaction temperature because of the low thermal stability of the H_2N−H_2BDC ligand.

TEM images in Figures 8 and S19−S24 indicate that the formed MIL-101(Cr)-NH_2 nanoparticles have a very small particle size, which matches well with their broad XRD diffraction peaks (see Figure 7a). However, significant particle agglomeration occurred at low temperatures of 110 and 120 °C, where particle aggregates larger than 100 nm are observed. Interestingly, particle agglomeration is suppressed by increasing the reaction temperature, and well-dispersed MIL-101(Cr)-NH_2 nanoparticles with small particle sizes of less than 20 nm are obtained at 140 °C. This finding likely relates to the improved ligand solubility and reaction kinetics for crystal formation at elevated temperatures. Further increasing the temperature to 150 °C and 160 °C results in severe agglomeration, likely due to enhanced particle collisions, and the formation of the amorphous phase. The BET surface areas of the MIL-101(Cr)-NH_2 particles show similar correlations with trends observed for particle sizes. As presented in Figures 7b and S25, the surface area continues to increase with

https://dx.doi.org/10.1021/acs.iecr.0c00535
Ind. Eng. Chem. Res. 2020, 59, 7888−7900

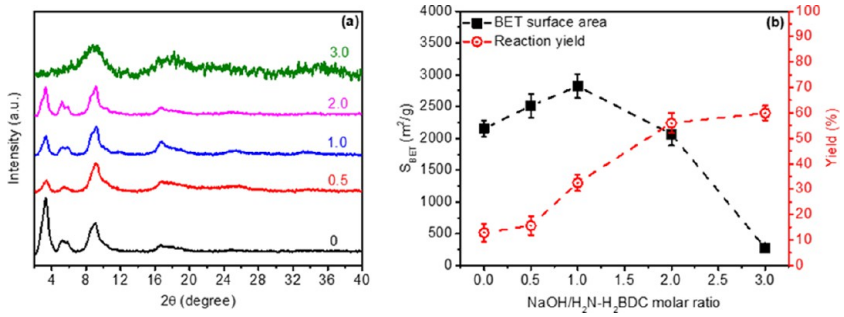

Figure 9. Powder XRD patterns (a) and BET surface areas and reaction yields (b) of MIL-101(Cr)-NH_2 nanoparticles synthesized at 140 °C for 24 h using a NaOH modulator with various NaOH/H_2N−H_2BDC molar ratios in water.

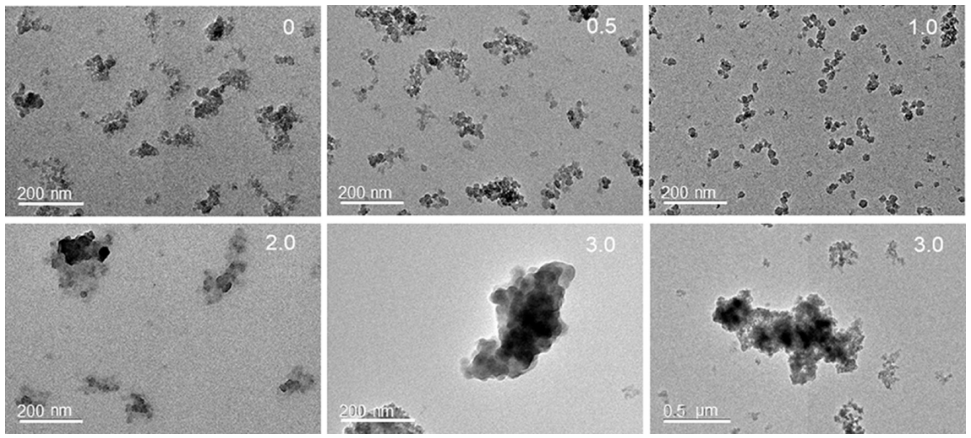

Figure 10. TEM images of MIL-101(Cr)-NH_2 nanoparticles synthesized at 140 °C for 24 h using a NaOH modulator with various NaOH/H_2N−H_2BDC molar ratios in water.

increased reaction temperature and reaches the highest value of 2800 ± 200 m^2/g at 140 °C before rapidly decreasing to around 2300 m^2/g at 150 °C and 160 °C. To the best of our knowledge, 2800 ± 200 m^2/g is the highest BET surface area for directly synthesized MIL-101(Cr)-NH_2 reported in the literature.

We further investigated the influence of NaOH concentration by adjusting the NaOH/H_2N−H_2BDC molar ratio while keeping the reaction temperature at 140 °C (see Table S2). The powder XRD patterns presented in Figure 9a suggest that MIL-101(Cr)-NH_2 could be formed at relatively low molar ratios of 2.0 or less, and a further increase of the molar ratio to 3.0 leads to the formation of an amorphous phase. Figures 9b and S26 show that there is a significant increase in reaction yield with the increase of NaOH/H_2N−H_2BDC molar ratio, while the BET surface area increases and reaches the highest value of 2800 ± 200 m^2/g at a molar ratio of 1.0 before dropping to 2000 ± 200 m^2/g at a molar ratio of 2.0. TEM images indicate that the NaOH/H_2N−H_2BDC molar ratio has a significant influence on particle morphology and size of the formed MIL-101(Cr)-NH_2 particles as well. As shown in Figures 10 and S27−S28, increasing the NaOH/H_2N−H_2BDC molar ratio from 0 to 1.0 leads to a reduction of particle size and agglomeration. Well-defined MIL-101(Cr)-NH_2 nanoparticles with a small particle size of less than 20 nm are obtained at a molar ratio of 1.0. In contrast, large particles with irregular shapes were formed at a higher molar ratio of 2.0, which correlates with a significant drop in the BET surface area. At an even higher molar ratio of 3.0, large aggregates and amorphous structures are observed (see Figures 10 and S29−S30), leading to a low surface area of 300 ± 50 m^2/g.

3.3. Effects of Base Modulator on MIL-101(Cr)-NH_2 Formation. As shown in Figure S31, the H_2N−H_2BDC ligand is slightly soluble in water at room temperature, forming a yellow-colored suspension. The addition of a NaOH modulator significantly increases the ligand solubility, where H_2N−H_2BDC fully dissolves in water at molar ratios of 2.0 and higher for NaOH/H_2N−H_2BDC. Such enhanced deprotonation of the carboxylic acids and solubility of the H_2N−H_2BDC provide more 2-aminoterephthalate ions to coordinate with the chromic metal ions, which significantly increases the reaction yields even at low reaction temperatures (see Figure 7b).

Given the increased ligand solubility with increasing amounts of NaOH, we followed the standard MIL-101(Cr)-NH_2 reaction procedure, but instead of heating the reaction solution to elevated temperatures as previously described, we carried out these reactions at room temperature. However, MIL-101(Cr)-NH_2 could not be formed under these conditions. Instead, we found that high NaOH loading resulted in the precipitation of a nonporous purple-gray-colored solid characterized by amorphous features and large aggregates. As illustrated in Figure S32, the H_2N−H_2BDC ligand is deprotonated by NaOH and thus soluble at a high NaOH/H_2N−H_2BDC molar ratio of 3.0, leaving a high concentration of 2-aminoterephthalate ions in water. When the $Cr(NO_3)_3$ metal precursor is then added to the solution, the purple-gray-colored solid precipitates immediately. XRD characterization reveals that the precipitated phase is not MIL-101(Cr)-NH_2. When the mixture was subsequently

https://dx.doi.org/10.1021/acs.iecr.0c00535
Ind. Eng. Chem. Res. 2020, 59, 7888−7900

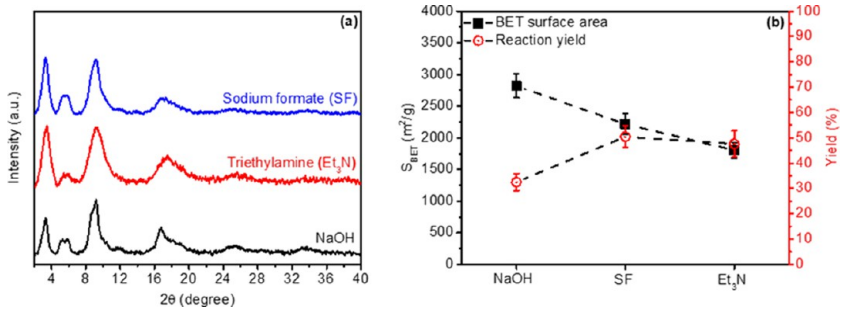

Figure 11. Powder XRD patterns (a) and BET surface areas and reaction yields (b) of MIL-101(Cr)-NH_2 synthesized at 140 °C for 24 h using different basic modulators with a base/H_2N−H_2BDC molar ratio of 1.0 in water.

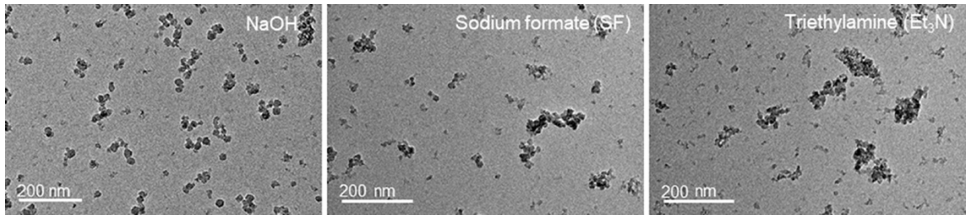

Figure 12. TEM images of MIL-101(Cr)-NH_2 nanoparticles synthesized at 140 °C for 24 h using different basic modulators with a base/H_2N−H_2BDC molar ratio of 1.0 in water.

reacted at 140 °C for 24 h, large aggregates with the same amorphous structure and low BET surface area were obtained as previously presented in Figures 9 and 10. This finding demonstrates the sensitive nature of using basic modulators to form MOFs from trivalent transition metals. Cr(III) readily forms metal oxides and metal hydroxides over a wide range of pH, and, hence, aqueous reaction conditions must be carefully controlled to enable the formation of a porous, crystalline MOF such as MIL-101(Cr)-NH_2.[43]

In addition to NaOH, organic bases including trimethylamine (Et_3N) and sodium formate (SF) were also considered to investigate the formation of MIL-101(Cr)-NH_2 particles. As shown in Figures 11 and S33, higher yields are achieved by using Et_3N- and SF-modulated reactions but the formed MIL-101(Cr)-NH_2 particles have lower surface areas compared to those synthesized using the NaOH modulator. The decline in surface area correlates with their larger particle size as shown in the TEM images (see Figures 12 and S34−S35). These findings imply that within the proper range of pH values, strong inorganic bases such as NaOH are excellent modulators to form high-quality MIL-101(Cr)-NH_2 nanoparticles with high surface area in water.

3.4. Characterization of the Synthesized MIL-101(Cr)-NH_2 Nanoparticles. Two MIL-101(Cr)-NH_2 samples with good crystallinity, small particle size, and high BET surface area were employed for further characterization. One sample was synthesized at 120 °C for 24 h in pure water (referred to as MIL-101(Cr)-NH_2) and the other was prepared at 140 °C for 24 h using a NaOH as the modulator with a NaOH/H_2N−H_2BDC molar ratio of 1.0 (referred to as MIL-101(Cr)-NH_2 (NaOH)). For comparison, the parent MIL-101(Cr) was synthesized as the benchmark.

Figures 13 and S36 show the morphology of two MIL-101(Cr)-NH_2 samples and the MIL-101(Cr) benchmark from TEM and SEM images. Clear differences exist in the particle morphology, particle size, and size uniformity. The MIL-101(Cr) shows the typical octahedral crystalline structure and relatively large particle size of hundreds of nanometers with a

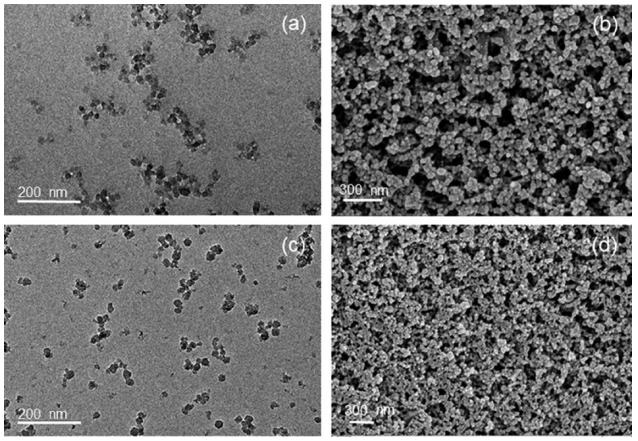

Figure 13. TEM and SEM images of MIL-101(Cr)-NH_2 synthesized at 120 °C for 24 h in pure water (a, b) and MIL-101(Cr)-NH_2 (NaOH) synthesized at 140 °C for 24 h using a NaOH modulator with a NaOH/H_2N−H_2BDC molar ratio of 1.0 in water (c, d).

broad particle size distribution.[15,36] In contrast, the two MIL-101(Cr)-NH_2 nanoparticles have a sphere-like morphology with ultrasmall particle sizes of less than 20 nm and good size uniformity. To the best of our knowledge, this is the smallest particle size reported in the literature for amine-functionalized MIL-101(Cr). Moreover, the spherical morphology is common for very small MOF nanoparticles that would otherwise have characteristic topographical features, such as the octahedral shape of the larger parent MIL-101(Cr).[15,33,44] As adsorbents, small particle sizes offer a larger external surface area and potentially more active surface sites for favorable gas adsorption capacity. When used as molecular sieving fillers in composite membranes, small particle sizes are important for reducing interfacial defects, agglomeration, and particle sedimentation to make mixed-matrix membranes (MMMs) that are highly selective.[45] This feature is critically important for forming industrially favorable membrane configurations with thin selective layers of several hundred nanometer

https://dx.doi.org/10.1021/acs.iecr.0c00535
Ind. Eng. Chem. Res. 2020, 59, 7888−7900

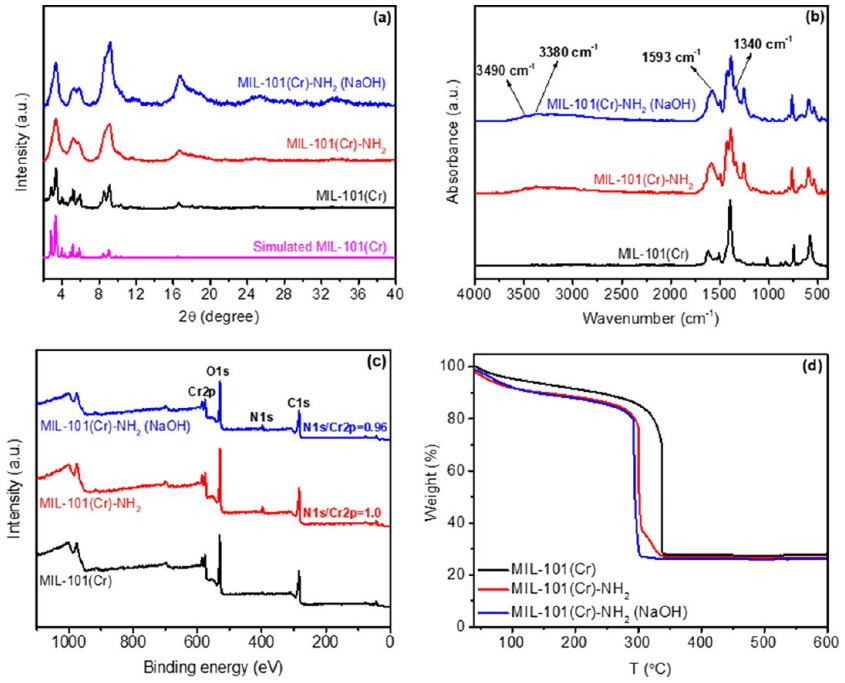

Figure 14. Powder XRD patterns (a), FTIR spectra (b), XPS analysis (c), and TGA curves (d) of MIL-101(Cr)-NH_2 synthesized at 120 °C for 24 h in pure water and MIL-101(Cr)-NH_2 (NaOH) synthesized at 140 °C for 24 h using a NaOH modulator with a NaOH/H_2N−H_2BDC molar ratio of 1.0 in water. The parent MIL-101(Cr) was used as a benchmark for comparison.

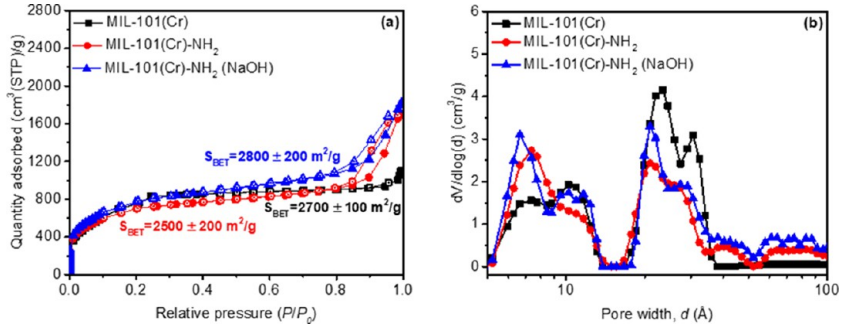

Figure 15. N_2 adsorption−desorption isotherms at 77 K and the calculated BET surface areas (a), and the pore size distribution curves with adsorption volume and pore width (b) of MIL-101(Cr)-NH_2 synthesized at 120 °C for 24 h and MIL-101(Cr)-NH_2 (NaOH) synthesized at 140 °C for 24 h using a NaOH modulator with a NaOH/H_2N−H_2BDC molar ratio of 1.0 in water. The parent MIL-101(Cr) was used as a benchmark for comparison. Adsorption is shown by filled symbols, and desorption is shown by open symbols.

thicknesses, and, thus, methods developed in this study may be useful for applications related to MMMs.

Powder XRD patterns in Figure 14a show that the positions of all diffraction peaks for the two MIL-101(Cr)-NH_2 samples are similar and match well with those for the MIL-101(Cr) benchmark and the simulated MIL-101 structure.[15] The rather broad diffraction peaks of the two MIL-101(Cr)-NH_2 samples suggest their small particle size, which is consistent with the observations from SEM and TEM. FTIR analysis in Figure 14b demonstrates the successful incorporation of amine functional groups into the MIL-101(Cr) framework, where the emerging double peaks at 3490 and 3380 cm^{-1} are ascribed to the asymmetric and symmetric vibrations of the $-NH_2$ groups, while the peaks at 1593 and 1340 cm^{-1} in the lower-frequency region correspond to the $-NH_2$ bending vibration and the $-C-NH_2$ stretching off of the phenyl ring, respectively.[33] XPS elemental analysis in Figure 14c also shows the existence of the N 1s peak at 399.2 eV in both MIL-101(Cr)-NH_2 samples, which we assigned to aromatic amines. In addition, the N/Cr atomic ratios for the two MIL-101(Cr)-NH_2 samples are approximately 1.0, which matches the theoretical value.[15] TGA was performed in air to evaluate the thermal stability of two MIL-101(Cr)-NH_2 samples. As presented in Figure 14d, two weight-loss steps are observed. The first step (~10%) occurs at temperatures lower than 150 °C and is attributed to the loss of atmospheric gases and water vapor that are adsorbed into the pores during benchtop sample preparation of MOFs for TGA experiments. The second step (~73%), mainly corresponding to the decomposition of the framework between 270 and 350 °C,[34] implies the excellent thermal stability of the MIL-101(Cr)-NH_2 nanoparticles.

N_2 adsorption−desorption isotherms at 77 K for the two MIL-101(Cr)-NH_2 samples and the MIL-101(Cr) benchmark were collected to determine their surface area, pore volume, and pore structure. As shown in Figure 15a, the two MIL-101(Cr)-NH_2 samples exhibited similar isotherms to that of the MIL-101(Cr) benchmark. All isotherms show a sharp uptake at P/P_0 values from 10^{-5} to 10^{-1}, which is a signature

https://dx.doi.org/10.1021/acs.iecr.0c00535
Ind. Eng. Chem. Res. 2020, 59, 7888−7900

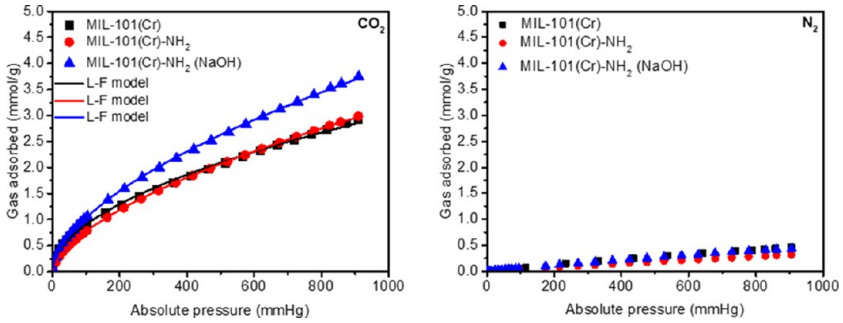

Figure 16. CO_2 and N_2 adsorption isotherms at 288 K for MIL-101(Cr)-NH_2 synthesized at 120 °C for 24 h and MIL-101(Cr)-NH_2 (NaOH) synthesized at 140 °C for 24 h using a NaOH modulator with a NaOH/H_2N−H_2BDC molar ratio of 1.0 in water. Points are experimental data, and solid lines are the fitted curves using the Langmuir−Freundlich (L−F) model. The parent MIL-101(Cr) was used as a benchmark for comparison.

feature of the microporous supertetrahedra.[46] The other two uptake steps near P/P_0 = 0.1 and P/P_0 = 0.2 reflect the presence of two kinds of nanoporous windows in the framework, while the increased N_2 uptake and the presence of hysteresis at high pressures are due to the textural interparticle pores created by the aggregated nanoparticles.[33] MIL-101(Cr)-NH_2 and MIL-101(Cr)-NH_2 (NaOH) possess apparent BET surface areas of 2500 ± 200 m^2/g and 2800 ± 200 m^2/g, respectively, which are comparable to that of the MIL-101(Cr) benchmark (2700 ± 100 m^2/g) but surpass those of other directly synthesized amine-functionalized MIL-101(Cr) MOFs. While one paper reports a surface area as high as 4100 m^2/g for MIL-101(Cr),[16] typical BET surface areas of MIL-101(Cr) are often in the range of 2500−3200 m^2/g.[17] The pore size distribution curves in Figure 15b display the two monodisperse pore sizes in MIL-101(Cr)-NH_2, which are slightly smaller than those in MIL-101(Cr) benchmark because of the addition of bulk amine groups onto the pore walls.

3.5. CO_2 and N_2 Adsorption Tests. The capability of the synthesized amine-functionalized MIL-101(Cr) nanoparticles for CO_2 capture was demonstrated by measuring their single gas adsorption isotherms for CO_2 and N_2 at different temperatures and pressures. These results are compared with those of the MIL-101(Cr) benchmark. A comprehensive study on their performance under more complex conditions, such as high pressures and humidified streams, is beyond the scope of this work and will be considered in a subsequent publication.

As shown in Figures 16 and S37, CO_2 exhibits much higher uptake than N_2 for all three MIL-101 samples in the range of tested pressures and temperatures due to the much stronger interaction of CO_2 with the framework. For example, MIL-101(Cr)-NH_2 (NaOH) shows a CO_2 uptake of 3.4 mmol/g at 750 mmHg and 288 K, while the MIL-101(Cr) benchmark has a much lower CO_2 uptake of 1.8 mmol/g. For postcombustion CO_2 capture, studies have investigated common adsorbents for pressure swings between 1.5 and 0.1 bar total pressures.[47,48] Assuming these conditions and ∼15 vol % CO_2, the CO_2 working capacity calculated from the isotherms in Figure 16 is approximately 5.1 wt % for MIL-101(Cr)-NH_2 (NaOH), which is about 1.4 times higher than that of the parent MIL-101(Cr) framework. These results indicate that performance improvements are possible for MIL-101(Cr) if functionalized variants with high surface area can be synthesized. At each temperature, the CO_2 uptake in the MIL-101(Cr)-NH_2 (NaOH) sample is much higher than that of the MIL-101(Cr) benchmark under the same pressure, while the MIL-101(Cr)-NH_2 sample shows similar CO_2 uptake values. This finding implies that obtaining a high surface area for the amine-functionalized MOF significantly enhances the CO_2 uptake.

Figures 16 and S37 also show that the N_2 uptakes in MIL-101(Cr)-NH_2 and MIL-101(Cr) benchmark are similar, suggesting that amine functionalization on the framework has a weak influence on N_2 adsorption. This finding can be explained by the different affinity of CO_2 and N_2 to amine groups. Theoretical models have demonstrated that the partially negative charge of the nitrogen in −NH_2 can interact favorably with the partially positive charge of the carbon in CO_2, and the acidic hydrogen atoms in −NH_2 can form hydrogen bonds with the oxygen atoms in CO_2.[35] As a result, more CO_2 than N_2 can adsorb as a result of the −NH_2 groups, which significantly increases the overall CO_2 adsorption capability. As a consequence, an excellent ideal CO_2/N_2 selectivity of up to 26.5 was achieved at 75 mmHg for MIL-101(Cr)-NH_2 (NaOH) even at a relatively high temperature of 308 K, which is 35% higher than that of the MIL-101(Cr) benchmark (see Table S4).

To further evaluate the influence of amine functionalization on CO_2 uptake, the CO_2 adsorption isotherms of MIL-101(Cr)-NH_2 (NaOH) and MIL-101(Cr) benchmark are replotted based on their per unit internal surface area. Using this normalization eliminates the slight differences in contribution from the different surface areas of each sample. As shown in Figure 17, the two MIL-101 MOFs show similar equilibrium CO_2 uptake per unit internal surface area at relatively low pressures of less than 200 mmHg. Above this pressure, the MIL-101(Cr)-NH_2 (NaOH) shows higher CO_2

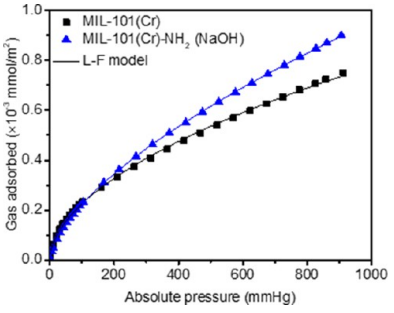

Figure 17. CO_2 adsorption isotherms on a per unit internal surface area basis at 308 K for (1) MIL-101(Cr)-NH_2 (NaOH) synthesized at 140 °C for 24 h in water using a NaOH modulator with a NaOH/H_2N−H_2BDC molar ratio of 1.0 and (2) the parent MIL-101(Cr) benchmark. Points are experimental data, and solid lines are the fitted curves by the Langmuir−Freundlich (L−F) model.

https://dx.doi.org/10.1021/acs.iecr.0c00535
Ind. Eng. Chem. Res. 2020, 59, 7888−7900

uptake than the parent MIL-101(Cr), and the difference becomes more significant with increasing pressure. This result suggests that there are distinct adsorption mechanisms at different pressures, where unsaturated chromium open metal sites (OMSs) likely dominate the adsorption of CO_2 at low pressures because of their strong affinity to the adsorbate, while the amine groups likely play a more important role at relatively high pressures when the OMSs become occupied.[49,50] This finding indicates that the added amine functionality improves CO_2 adsorption in MIL-101(Cr)-NH_2 (NaOH) by providing secondary adsorption sites that more favorably interact with CO_2 than those of the parent MIL-101(Cr) framework. From an application perspective, it is well known that OMSs are particularly susceptible to water in wet flue gas.[51] Therefore, an inherent benefit to amine functionalization is that improvements in working capacity can be attributed to modifications of secondary binding sites, which do not contain OMSs. Moreover, from the perspective of membrane-based separations, which are steady-state operations, an improvement in CO_2 adsorption is expected to also contribute to increased permeability,[52] and amine functionalization presents an opportunity to adapt previous inaccessible yet highly desirable compatibilization strategies such as postsynthetic modification (PSM). PSM of related materials can be used to form MMMs with compatible interfaces[53] and may also be used to attach polymer binders to the MOF for effective pelletization strategies to form adsorbents.

The isosteric heats (Q_{st}) for CO_2 adsorption of the amine-functionalized MIL-101(Cr) samples were calculated using the Clausius–Clapeyron equation to better quantify the role of the amine on CO_2–framework interactions. The amount of CO_2 adsorbed at a given pressure was estimated from a fit to the Langmuir–Freundlich model for the three isotherms shown in Figures 16 and S37. As shown in Figure 18, the infinite dilution

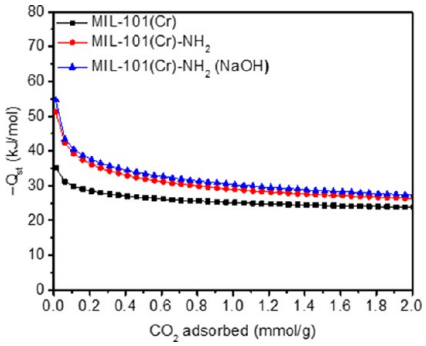

Figure 18. Isosteric heats (Q_{st}) of CO_2 adsorption in MIL-101(Cr)-NH_2 synthesized at 120 °C for 24 h in pure water and MIL-101(Cr)-NH_2 (NaOH) synthesized at 140 °C for 24 h using a NaOH modulator with a NaOH/H_2N–H_2BDC molar ratio of 1.0 in water. The parent MIL-101(Cr) was used as a benchmark for comparison.

Q_{st} values are around −51.2 and −54.6 kJ/mol for MIL-101(Cr)-NH_2 and MIL-101(Cr)-NH_2 (NaOH), respectively, which are among some of the highest values for amine-functionalized MOFs reported in the literature.[54−57] In contrast, the MIL-101(Cr) benchmark shows a lower Q_{st} of approximately −35.1 kJ/mol due to its milder affinity with CO_2. With increasing pressure, CO_2 adsorption becomes less favorable as the primary and secondary binding sites are saturated, and thus the adsorbate–adsorbent interactions become weaker. As a result, the Q_{st} values become less negative and begin to approach similar values with increasing pressure for all samples considered. The isosteric heats together with the adsorption performance imply that the superior CO_2 uptake in the amine-functionalized MIL-101(Cr) is ascribed to the strong interaction between CO_2 and the basic amine functionality.

4. CONCLUSIONS

Hydrothermal reactions of chromic(III) nitrate and 2-aminoterephthalic acid were systematically studied to directly synthesize high-quality amine-functionalized MIL-101(Cr) nanoparticles. Important reaction trends were extracted to investigate how various synthesis parameters and basic modulators influence particle quality. It was observed that the reaction temperature and time play an important role in MOF crystal formation, while the influence of reactant concentration is of marginal importance because of the low solubility of the ligand in water, which appears to be the rate-limiting step for particle growth. The addition of a basic modulator such as NaOH promoted the dissociation of 2-aminoterephthalic acid and thus significantly increased ligand solubility in water, which improved the reaction yield and the particle surface area. However, an amorphous phase appears when the molar ratio of NaOH/2-aminoterephthalic acid is higher than 2.0, leading to a significant loss in surface area. This finding demonstrates the sensitive nature of using basic modulators to form MOFs from trivalent transition metals. An optimized recipe to synthesize amine-functionalized MIL-101(Cr) nanoparticles was determined to form MIL-101(Cr)-NH_2 with small particle sizes of less than 20 nm, a high BET surface area of 2800 ± 200 m^2/g, excellent CO_2 adsorption of up to 3.4 mmol/g at 288 K, and high CO_2/N_2 selectivity of 26.5 at 308 K. A high Q_{st} value of −54.6 kJ/mol for CO_2 adsorption implies a strong interaction between CO_2 and the basic amine. The development of high-quality sub-20 nm amine-functionalized MIL-101(Cr) nanoparticles provides a facile and effective strategy to synthesize MIL-101(Cr)-based materials for CO_2 capture.

■ ASSOCIATED CONTENT

Supporting Information

The Supporting Information is available free of charge at https://pubs.acs.org/doi/10.1021/acs.iecr.0c00535.

Additional TEM images; XRD patterns; N_2 adsorption–desorption isotherms at 77 K; images of particle suspension in ethanol; and CO_2, CH_4, and N_2 adsorption isotherms at 288 and 298 K (PDF)

■ AUTHOR INFORMATION

Corresponding Author

Zachary P. Smith − *Department of Chemical Engineering, Massachusetts Institute of Technology, Cambridge, Massachusetts 02139, United States;* orcid.org/0000-0002-9630-5890; Phone: +1 6177154503; Email: zpsmith@mit.edu; Fax: +1 6172588224

Authors

Gang Han − *Department of Chemical Engineering, Massachusetts Institute of Technology, Cambridge, Massachusetts 02139, United States*

https://dx.doi.org/10.1021/acs.iecr.0c00535
Ind. Eng. Chem. Res. 2020, 59, 7888−7900

Qihui Qian − *Department of Chemical Engineering, Massachusetts Institute of Technology, Cambridge, Massachusetts 02139, United States*
Katherine Mizrahi Rodriguez − *Department of Chemical Engineering, Massachusetts Institute of Technology, Cambridge, Massachusetts 02139, United States*

Complete contact information is available at: https://pubs.acs.org/10.1021/acs.iecr.0c00535

Notes

The authors declare no competing financial interest.

■ ACKNOWLEDGMENTS

The authors gratefully acknowledge the financial support from the Abdul Latif Jameel Water and Food Systems Lab (J-WAFS) at MIT. Special thanks are also due to Dr. Moonjoo Lee, Dr. Won Seok Chi, Dr. Francesco M. Benedetti, Albert Wu, Patrick Asinger, Taigyu Joo, Sharon Lin, Hyunhee Lee, and Shiqi Zhao for their valuable help and suggestions.

■ REFERENCES

(1) Long, J. R.; Yaghi, O. M. The Pervasive Chemistry of Metal−Organic Frameworks. *Chem. Soc. Rev.* **2009**, *38*, 1213−1214.
(2) Jiang, J.; Zhao, Y.; Yaghi, O. M. Covalent Chemistry beyond Molecules. *J. Am. Chem. Soc.* **2016**, *138*, 3255−3265.
(3) Zhou, H. C.; Long, J. R.; Yaghi, O. M. Introduction to Metal−Organic Frameworks. *Chem. Rev.* **2012**, *112*, 673−674.
(4) Furukawa, H.; Cordova, K. E.; ÓKeeffe, M.; Yaghi, O. M. The Chemistry and Applications of Metal−Organic Frameworks. *Science* **2013**, *341*, No. 1230444.
(5) Chughtai, A. H.; Ahmad, N.; Younus, H. A.; Laypkovc, A.; Verpoort, F. Metal−Organic Frameworks: Versatile Heterogeneous Catalysts for Efficient Catalytic Organic Transformations. *Chem. Soc. Rev.* **2015**, *44*, 6804−6849.
(6) Li, L.; He, J.; Wang, Y.; Lv, X.; Gu, X.; Dai, P.; Liu, D.; Zhao, X. Metal−Organic Frameworks: A Promising Platform for Constructing Non-Noble Electrocatalysts for the Oxygen Reduction Reaction. *J. Mater. Chem. A* **2019**, *7*, 1964−1988.
(7) Della Rocca, J.; Liu, D.; Lin, W. Nanoscale Metal-Organic Frameworks for Biomedical Imaging and Drug Delivery. *Acc. Chem. Res.* **2011**, *44*, 957−968.
(8) McKinlay, A. C.; Morris, R. E.; Horcajada, P.; Férey, G.; Gref, R.; Couvreur, P.; Serre, C. Biomofs: Metal−Organic Frameworks for Biological and Medical Applications. *Angew. Chem., Int. Ed.* **2010**, *49*, 6260−6266.
(9) Hu, Z.; Deibert, B. J.; Li, J. Luminescent Metal−Organic Frameworks for Chemical Sensing and Explosive Detection. *Chem. Soc. Rev.* **2014**, *43*, 5815−5840.
(10) Li, H.; Wang, K.; Sun, Y.; Lollar, C. T.; Li, J.; Zhou, H. C. Recent Advances in Gas Storage and Separation Using Metal−Organic Frameworks. *Mater. Today* **2018**, *21*, 108−121.
(11) Herm, Z. R.; Bloch, E. D.; Long, J. R. Hydrocarbon Separations in Metal−Organic Frameworks. *Chem. Mater.* **2014**, *26*, 323−338.
(12) Adil, K.; Belmabkhout, Y.; Pillai, R. S.; Cadiau, A.; Bhatt, P. M.; Assen, A. H.; Maurin, G.; Eddaoudi, M. Gas/Vapour Separation Using Ultra-Microporous Metal−Organic Frameworks: Insights into the Structure/Separation Relationship. *Chem. Soc. Rev.* **2017**, *46*, 3402−3430.
(13) Park, J.; Lively, R. P.; Sholl, D. S. Establishing Upper Bounds on CO_2 Swing Capacity in Sub-Ambient Pressure Swing Adsorption via Molecular Simulation of Metal−Organic Frameworks. *J. Mater. Chem. A* **2017**, *5*, 12258−12265.
(14) Férey, G.; Serre, C.; Mellot-Draznieks, C.; Millange, F.; Surblé, S.; Dutour, J.; Margiolaki, I. A Hybrid Solid with Giant Pores Prepared by a Combination of Targeted Chemistry, Simulation, and Powder Diffraction. *Angew. Chem., Int. Ed.* **2004**, *43*, 6296−6301.
(15) Férey, G.; Mellot-Draznieks, C.; Serre, C.; Millange, F.; Dutour, J.; Surblé, S.; Margiolaki, I. A Chromium Terephthalate-Based Solid with Unusually Large Pore Volumes and Surface Area. *Science* **2005**, *309*, 2040−2042.
(16) Hong, D. Y.; Hwang, Y. K.; Serre, C.; Férey, G.; Chang, J. S. Porous Chromium Terephthalate MIL-101 with Coordinatively Unsaturated Sites: Surface Functionalization, Encapsulation, Sorption and Catalysis. *Adv. Funct. Mater.* **2009**, *19*, 1537−1552.
(17) Bhattacharjee, S.; Chen, C.; Ahn, W. S. Chromium Terephthalate Metal−Organic Framework MIL-101: Synthesis, Functionalization, and Applications for Adsorption and Catalysis. *RSC Adv.* **2014**, *4*, 52500−52525.
(18) Munusamy, K.; Sethia, G.; Patil, D. V.; Rallapalli, P. B. S.; Somani, R. S.; Bajaj, H. C. Sorption of Carbon Dioxide, Methane, Nitrogen and Carbon Monoxide on MIL-101(Cr): Volumetric Measurements and Dynamic Adsorption Studies. *Chem. Eng. J.* **2012**, *195*−*196*, 359−368.
(19) Ma, J.; Ying, Y.; Guo, X.; Huang, H.; Liu, D.; Zhong, C. Fabrication of Mixed-Matrix Membrane Containing Metal−Organic Framework Composite with Task Specific Ionic Liquid for Efficient CO_2 Separation. *J. Mater. Chem. A* **2016**, *4*, 7281−7288.
(20) Maksimchuk, N. V.; Zalomaeva, O. V.; Skobelev, I. Y.; Kovalenko, K. A.; Fedin, V. P.; Kholdeeva, O. A. Metal−Organic Frameworks of the MIL-101 Family as Heterogeneous Singlesite Catalysts. *Proc. R. Soc., A* **2012**, *468*, 2017−2034.
(21) Yang, Y.; Lin, R.; Ge, L.; Hou, L.; Bernhardt, P.; Rufford, T. E.; Wang, S.; Rudolph, V.; Wang, Y.; Zhu, Z. Synthesis and Characterization of Three Aminofunctionalized Metal−Organic Frameworks Based on The 2-Aminoterephthalic Ligand. *Dalton Trans.* **2015**, *44*, 8190−8197.
(22) Emerson, A. J.; Chahine, A.; Batten, S. R.; Turner, D. R. Synthetic Approaches for The Incorporation of Free Amine Functionalities in Porous Coordination Polymers for Enhanced CO_2 Sorption. *Coord. Chem. Rev.* **2018**, *365*, 1−22.
(23) Wang, X.; Li, H.; Hou, X. J. Amine-Functionalized Metal Organic Framework as A Highly Selective Adsorbent for CO_2 Over CO. *J. Phys. Chem. C* **2012**, *116*, 19814−19821.
(24) Joshi, J. N.; Zhu, G.; Lee, J. J.; Carter, E. A.; Jones, C. W.; Lively, R. P.; Walton, K. S. Probing Metal−Organic Framework Design for Adsorptive Natural Gas Purification. *Langmuir* **2018**, *34*, 8443−8450.
(25) Zhou, F.; Zhou, J.; Gao, X.; Kong, C.; Chen, L. Facile Synthesis of MOFs with Uncoordinated Carboxyl Groups for Selective CO_2 Capture via Postsynthetic Covalent Modification. *RSC Adv.* **2017**, *7*, 3713−3719.
(26) Luan, Y.; Qi, Y.; Gao, H.; Andriamitantsoa, R. S.; Zheng, N.; Wang, G. A General Postsynthetic Modification Approach of Amino-Tagged Metal−Organic Frameworks to Access Efficient Catalysts for the Knoevenagel Condensation Reaction. *J. Mater. Chem. A* **2015**, *3*, 17320−17331.
(27) Lee, Y. R.; Yu, K.; Ravi, S.; Ahn, W. S. Selective Adsorption of Rare Earth Elements Over Functionalized Cr-MIL-101. *ACS Appl. Mater. Interfaces* **2018**, *10*, 23918−23927.
(28) Wang, Z.; Cohen, S. M. Modification of A Neutral Metal-Organic Framework. *J. Am. Chem. Soc.* **2007**, *129*, 12368−12369.
(29) Shaabani, A.; Mohammadian, R.; Hashemzadeh, A.; Afshari, R.; Amini, M. M. Aminefunctionalized MIL-101(Cr) Embedded with Co(II) Phthalocyanine as A Durable Catalyst for One-Pot Tandem Oxidative A^3 Coupling Reactions of Alcohols. *New J. Chem.* **2018**, *42*, 4167−4174.
(30) Yin, Z.; Wan, S.; Yang, J.; Kurmoo, M.; Zeng, M. H. Recent Advances in Post-Synthetic Modification of Metal−Organic Frameworks: New Types and Tandem Reactions. *Coord. Chem. Rev.* **2019**, *378*, 500−512.
(31) Li, X.; Mao, Y.; Leng, K.; Ye, G.; Sun, Y.; Xu, W. Synthesis of Amino-Functionalized MIL-101(Cr) with Large Surface Area. *Mater. Lett.* **2017**, *197*, 192−195.
(32) Bauer, S.; Serre, C.; Devic, T.; Horcajada, P.; Marrot, J.; Férey, G.; Stock, N. Highthroughput Assisted Rationalization of the

Formation of Metal Organic Frameworks in the Iron(Iii) Amino-terephthalate Solvothermal System. *Inorg. Chem.* **2008**, *47*, 7568−7576.
(33) Lin, Y.; Kong, C.; Chen, L. Direct Synthesis of Amine-Functionalized MIL-101(Cr) Nanoparticles and Application for CO_2 Capture. *RSC Adv.* **2012**, *2*, 6417−6419.
(34) Jiang, D.; Keenan, L. L.; Burrows, A. D.; Edler, K. J. Synthesis and Post-Synthetic Modification of MIL-101(Cr)-NH_2 via A Tandem Diazotisation Process. *Chem. Commun.* **2012**, *48*, 12053−12055.
(35) Zhang, K.; Chen, Y.; Nalaparaju, A.; Jiang, J. Functionalized Metal−Organic Framework MIL-101 for CO_2 Capture: Multi-Scale Modeling from ab Initio Calculation and Molecular Simulation to Breakthrough Prediction. *CrystEngComm* **2013**, *15*, 10358−10366.
(36) Bromberg, L.; Diao, Y.; Wu, H.; Speakman, S. A.; Hatton, T. A. Chromium(III) Terephthalate Metal Organic Framework (MIL-101): HF-Free Synthesis, Structure, Polyoxometalate Composites, and Catalytic Properties. *Chem. Mater.* **2012**, *24*, 1664−1675.
(37) Zhou, X.; Huang, W.; Miao, J.; Xia, Q.; Zhang, Z.; Wang, H.; Li, Z. Enhanced Separation Performance of A Novel Composite Material Gro@MIL-101 for CO_2/CH_4 Binary Mixture. *Chem. Eng. J.* **2015**, *266*, 339−344.
(38) Chen, C.; Feng, N.; Guo, Q.; Li, Z.; Li, X.; Ding, J.; Wang, L.; Wan, H.; Guan, G. Templatedirected Fabrication of MIL-101(Cr)/Mesoporous Silica Composite: Layer-Packed Structure and Enhanced Performance for CO_2 Capture. *J. Colloid Interface Sci.* **2018**, *513*, 891−902.
(39) Kayal, S.; Chakraborty, A. Impact of Alkali-Metal Impregnation on MIL-101 (Cr) Metal−Organic Frameworks for CH_4 and CO_2 Adsorption Studies. *ChemPhysChem* **2018**, *19*, 3158−3165.
(40) Huang, Y. H.; Lo, W. S.; Kuo, Y. W.; Chen, W. J.; Lin, C. H.; Shieh, F. K. Green and Rapid Synthesis of Zirconium Metal−Organic Frameworks via Mechanochemistry: UiO-66 Analog Nanocrystals Obtained in One Hundred Seconds. *Chem. Commun.* **2017**, *53*, 5818−5821.
(41) Guo, H.; Zhu, Y.; Wang, S.; Su, S.; Zhou, L.; Zhang, H. Combining Coordination Modulation with Acid−Base Adjustment for the Control Over Size of Metal−Organic Frameworks. *Chem. Mater.* **2012**, *24*, 444−450.
(42) Xin, C.; Zhan, H.; Huang, X.; Li, H.; Zhao, N.; Xiao, F.; Wei, W.; Sund, Y. Effect of Various Alkaline Agents on the Size and Morphology of Nano-Sized HKUST-1 for CO_2 Adsorption. *RSC Adv.* **2015**, *5*, 27901−27911.
(43) Yaghi, O. M.; Kalmutzki, M. J.; Diercks, C. S. *Introduction to Reticular Chemistry: Metal-Organic Frameworks and Covalent Organic Frameworks*; John Wiley and Sons: Weinheim, 2019; p 552. ISBN 978-3-527-82110-5.
(44) Jiang, D.; Burrows, A. D.; Edler, K. J. Size-Controlled Synthesis of MIL-101 (Cr) Nanoparticles with Enhanced Selectivity for CO_2 over N_2. *CrystEngComm* **2011**, *13*, 6916−6919.
(45) Lin, R.; Hernandez, B. V.; Ge, L.; Zhu, Z. Metal Organic Framework Based Mixed Matrix Membranes: An Overview on Filler/Polymer Interfaces. *J. Mater. Chem. A* **2018**, *6*, 293−312.
(46) Côté, A. P.; Benin, A. I.; Ockwig, N. W.; ÓKeefe, M.; Matzger, A. J.; Yaghi, O. M. Porous, Crystalline, Covalent Organic Frameworks. *Science* **2005**, *310*, 1166−1170.
(47) Riboldi, L.; Bolland, O. Overview on Pressure Swing Adsorption (PSA) as CO_2 Capture Technology: State-of-the-Art, Limits and Potentials. *Energy Procedia* **2017**, *114*, 2390−2400.
(48) Hu, Z.; Wang, Y.; Shah, B. B.; Zhao, D. CO_2 Capture in Metal−Organic Framework Adsorbents: An Engineering Perspective. *Adv. Sustainable Syst.* **2019**, *3*, No. 1800080.
(49) Chowdhury, P.; Mekala, S.; Dreisbach, F.; Gumma, S. Adsorption of CO, CO_2 and CH_4 on Cu-BTC and MIL-101 Metal Organic Frameworks: Effect of Open Metal Sites and Adsorbate Polarity. *Microporous Mesoporous Mater.* **2012**, *152*, 246−252.
(50) Hou, X. J.; Li, H.; He, P. Theoretical Investigation for Adsorption of CO_2 and CO on MIL-101 Compounds with Unsaturated Metal Sites. *Comput. Theor. Chem.* **2015**, *1055*, 8−14.
(51) Boyd, P. G.; Chidambaram, A.; García-Díez, E.; Ireland, C. P.; Daff, T. D.; Bounds, R.; Gładysiak, A.; Schouwink, P.; Moosavi, S. M.; Maroto-Valer, M. M.; Reimer, J. A.; Navarro, J. A. R.; Woo, T. K.; Garcia, S.; Stylianou, K. C.; Smit, B. Data-Driven Design of Metal−Organic Frameworks for Wet Flue Gas CO_2 Capture. *Nature* **2019**, *576*, 253−256.
(52) Li, C.; Meckler, S. M.; Smith, Z. P.; Bachman, J. E.; Maserati, L.; Long, J. R.; Helms, B. A. Engineered Transport in Microporous Materials and Membranes for Clean Energy Technologies. *Adv. Mater.* **2018**, *30*, No. 1704953.
(53) Qian, Q.; Wu, A. X.; Chi, W. S.; Asinger, P. A.; Lin, S.; Hypsher, A.; Smith, Z. P. Mixed-Matrix Membranes Formed from Imide-Functionalized UiO-66-NH2 for Improved Interfacial Compatibility. *ACS Appl. Mater. Interfaces* **2019**, *11*, 31257−31269.
(54) Vaidhyanathan, R.; Iremonger, S. S.; Shimizu, G. K. H.; Boyd, P. G.; Alavi, S.; Woo, T. K. Competition and Cooperativity in Carbon Dioxide Sorption by Amine-Functionalized Metal−Organic Frameworks. *Angew. Chem., Int. Ed.* **2012**, *51*, 1826−1829.
(55) Caskey, S. R.; Wong-Foy, A. G.; Matzger, A. J. Dramatic Tuning of Carbon Dioxide Uptake via Metal Substitution in A Coordination Polymer with Cylindrical Pores. *J. Am. Chem. Soc.* **2008**, *130*, 10870−10871.
(56) Vaidhyanathan, R.; Iremonger, S. S.; Dawson, K. W.; Shimizu, G. K. H. An Aminefunctionalized Metal Organic Framework for Preferential CO_2 Adsorption at Low Pressures. *Chem. Commun.* **2009**, *35*, 5230−5232.
(57) Lin, Y.; Kong, C.; Chen, L. Amine-Functionalized Metal−Organic Frameworks: Structure, Synthesis and Applications. *RSC Adv.* **2016**, *6*, 32598−32614.

https://dx.doi.org/10.1021/acs.iecr.0c00535
Ind. Eng. Chem. Res. 2020, 59, 7888−7900